RSC Advances

ROYAL SOCIETY OF CHEMISTRY

www.rsc.org/advances

Cite this: DOI: 10.1039/c0xx00000x

www.rsc.org/xxxxxx

ARTICLE TYPE

Enhanced performance of poly (ether sulfone) based composite proton exchange membranes with sulfonated polymer brush functionalized graphene oxide

Yanxu Zhao [a], Yuqin Fu *[b], Yao He [a], Bo Hu [a], Lingdi Liu [a], Jianhua Lü[a] and Changli Lü*[a]

Received (in XXX, XXX) Xth XXXXXXXXX 20XX, Accepted Xth XXXXXXXXX 20XX
DOI: 10.1039/b000000x

Sulfonated polymer brush functionalized graphene oxide (SPB-FGO) was prepared by reversible addition fragmentation chain transfer (RAFT) polymerization, and then was introduced into sulfonated poly(ether sulfone) (SPES) matrix to fabricate composite proton exchange membranes (PEMs). The influence of loading content of SPB-FGO on the properties of the composite membranes was intensively studied. It was demonstrated that the properties including proton conductivity, thermal stability, mechanical property and oxidative stability for the composite membranes were improved as compared with that of pristine SPES membrane. Meanwhile, the methanol permeability of composite membranes was lower than that of the pristine membrane. The proton conductivity of SPES/SPB-FGO-2 was nearly two times increase as compared with that of the pristine membrane at 25 ^{o}C. This result could be attributed to that the SPB-FGO was well-distributed within the SPES membrane matrix and the ion clusters were relatively uniform in size, which made SPB-FGO fillers create broad ionic pathways through the sulfonic acid groups in polymer brushes via interfacial interactions. Our study demonstrated that the incorporation of proper content of SPB-FGOs could improve the properties of PEMs, opening up a new design concept to fabricate organic-inorganic composite PEMs.

1. Introduction

Fuel cells, which can convert chemical energy directly into electrical energy, have attracted great attention because of the high conversion rate, low environment pollution and low noise.[1,2] Among the fuel cells, the proton exchange membrane fuel cells (PEMFCs) have been widely studied. The proton exchange membrane (PEM), a core material of PEMFCs, serves as the conducting medium of the proton and the separator of anode and cathode, determines the efficiency and durability of PEMFCs. At present, Nafion is the state-of-the-art PEM due to its good chemical stability, high mechanical strength as well as high proton conductive ability. Nevertheless, this type of PEM has some disadvantages such as limited operation temperature (< 80 ^{o}C), high cost and high methanol permeability.[3] In view of these disadvantages, researchers have attempted to modify the Nafion membrane or prepare other membranes with better performance to make their applications in the PEMFCs.[4-7]

At present, the composite PEMs have been also developed by different methods including organic-inorganic hybridization, organic-organic hybridization, membrane crosslinking, layer-by-layer assembly and so on.[8-10] In these methods, organic-inorganic hybridization method is the most widely used. The introduction of inorganic fillers can enhance the membrane properties such as mechanical strength, thermal ability and reduced swelling etc.[11-13] As is known to all, graphene, as a thinnest nanomaterial in the world, has high electronic mobility, low resistivity and high conductive speed.[14] The graphene oxide (GO) can be effectively functionalized due to its large number of surface functional groups. Therefore, the modified GO has been used to enhance the properties of the composite PEMs. Several recent reports have been demonstrated that the incorporation of GO in polymer matrix to fabricate the organic-inorganic nanocomposite membranes is a promising approach for the modification of PEMs.[15,16] Choi et al.[15] found that when GO was introduced into Nafion membrane, the microstructure of Nafion membrane was altered and the composite membranes showed outstanding mechanical properties. Wang et al.[16] prepared a new type of graphene oxide (GO)/Nafion composite membranes via layer-by-layer (LbL) procedure. The composite membranes exhibited improved oxidative stability, lower methanol permeability and higher selectivity. In order to enhance the compatibility between GO and host materials,[17-19] the GO's surface functional groups were modified by small molecules and polymer containing sulfonic acid groups, and then the modified GO sheets were introduced to the polymer matrix to fabricate PEMs.[20-23] Feng et al.[21] prepared the composite membranes by introducing S-GO-SiO_2 into Nafion matrix and S-GO-SiO_2 had a good dispersibility inside the membrane matrix. The proton conductivity of composite membrane with 0.1 wt % S-GO-SiO_2 increased nearly two times as compared with that of pristine membrane. Zhao et al.[22] prepared the composite membranes by introducing the sulfonated polymer brush modified GO into SPEEK matrix. The proton conductivity of SPEEK/SSGO-10 was 123% of that of SPEEK control membrane. It was found that the SP-GO fillers were uniformly dispersed within the membranes. Sharma et al.[23] introduced the modified GO into the sulfonated chitosan polymer

matrix to prepare the biopolymer PEMs. The proton conductivity of MGO-SCH-5 composite membrane was nearly two times of that of the pristine membrane. The composite membranes showed better thermal stabilities and mechanical properties. Therefore, the polymer modified GO as the inorganic fillers is a promising strategy to fabricate PEMs to further enhance the compatibility between GO and host materials, which can further improve the properties of the resulting composite PEMs.

According to the extensive reports,[24,25] only the available functional groups can provide proton transfer sites to improve the proton conductivity. As a consequence, many effective groups are adopted to improve the proton conductivity. One facile and efficient approach to increase the loading amount of functional groups is to coat a polymer layer on the surface of inorganic fillers. Presently, the polymer layer is composed of two types with the different structures: one is mainly based on the cross-linked polymer layer;[26,27] the other is "brush-like layer" formed by grafting linear polymer.[22,28] By comparison, the brush-like layer has the following advantages: (I) better contact with the polymer matrix, so as to improve the compatibility and dispersity;[29] (II) better chain motion of linear polymer than cross-linked polymer, which can lower energy barrier for proton hopping. Zhao et al.[22] have introduced sulfonated polymer brush modified GO into SPEEK matrix to improve the properties of SPEEK membranes. Zhang et al.[28] introduced the hollow polymer microspheres grafted with sulfonated polystyrene brushes into SPEEK matrix. The conductivity of the composite membrane with 15 wt % inorganic filler could reach 0.33 S cm^{-1}, while the proton conductivity of the pristine membrane was 0.18 S cm^{-1} at 75 ^{o}C.

At present, the preparation methods of polymer functionalized GO generally have two kinds: "grafting to" and "grafting from". Relatively, the "grafting from" method is better than the "grafting to" method because this functionalized strategy can improve the solubility of the material. So the resulting materials can be further modified or chemically characterized. In addition, the polymer chains can grow from the modified GO sheets to achieve excellent control over the density.[30-32] At present, atom transfer radical polymerization (ATRP)[33,34] and reversible addition fragmentation chain transfer (RAFT)[35,36] polymerization are the two types of usual surface-initiated polymerization methods. Ohno et al.[33] succeeded in preparing silica particles with a shell layer of a well-defined poly (methyl methacrylate) (PMMA) brush. However, ATRP polymerization requires the use of a metal catalyst and a ligand, which may contaminate the product. RAFT polymerization is a kind of active controlled radical polymerization and has been widely used because its reaction condition is easier to implement and synthetic operation is simpler. Through RAFT polymerization, the perfectly dispersive and highly uniform hybrid particles grafted with polymer brushes can be produced.[35] Here, we try to introduce the polymer brush functionalized GO into the polyelectrolyte membranes to prepare the composite PEMs. The "grafting from" method based on the RAFT polymerization was used in this article. The monomer of sodium-p-styrenesulfonate was grafted from the surface of the GO successfully to obtain the polymer brush functionalized GO with high proton conductivity.

As for the polymer matrix, we try to find fuel cell membrane materials with better comprehensive properties. At present, the aromatic polymer acid type membranes are widely used in fuel cells, including sulfonated polyimide,[37,38] sulfonated poly(ether sulfone),[39-42] sulfonated polybenzimidazol[43,44] and sulfonated poly(ether ether ketone).[45,46] Among the various polymers, we adopted poly(ether sulfone) with fluorene chain segment as polymer matrix due to the good chemical stability and thermal stability of the fluorine chain segment.[47-49]

Here, we prepared a series of novel polymer composite PEMs based on sulfonated poly(ether sulfone) (SPES) and sulfonated polymer brush functionalized GO (SPB-FGO) via a simple blending method. As shown in Scheme 1, the GO sheets were firstly functionalized with an alkoxylsilane (APTES) to obtain the amine group modified GO (A-GO). The amino groups of A-GO reacted with carboxyl groups of DDAT to obtain RAFT agent functionalized GO (A-FGO). Then the AIBN initiated RAFT polymerization of sodium-p-styrenesulfonate (SS) from the surface of A-FGO to get SPB-FGO. Finally, different amounts of SPB-FGO were incorporated into SPES with good thermal stability and chemical stability to fabricate the composite PEMs. The SPB-FGO was utilized to enhance the proton conductivity and water uptake due to the hydrophilic sulfonic acid groups on SPB-FGO. The influences of the content of SPB-FGO on the membrane properties including microstructure, thermal stability, mechanical property, methanol permeability and other properties are all determined and discussed.

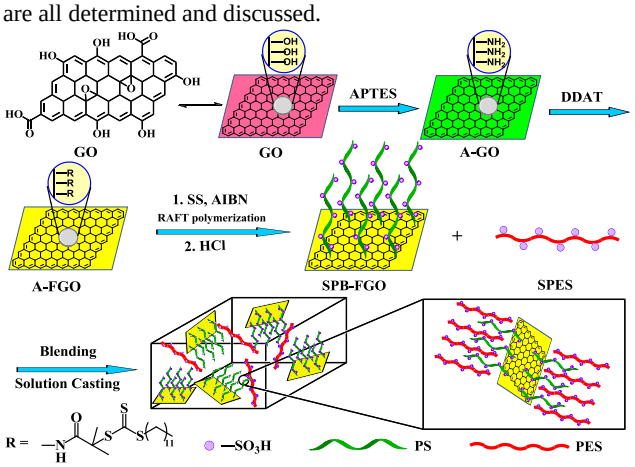

Scheme 1 Schematic diagram of the synthesis of polymer brush functionalized graphene oxide (SPB-FGO) from GO and the microstructure of hybrid composite membranes.

2. Experimental

2.1 Materials

Graphite powders (45 μm) were purchased from Shandong Qingdao Laixi Graphite Company in China. 3-Amino-propyltriethoxysilane (APTES) and sodium-p-styrenesulfonate (SS) (before use, it was recrystallized twice from the mixture of ethanol and deionized water at 60 ^{o}C) were purchased from Aladdin. S-1-Dodecyl-S´-(α,α´-dimethyl-α´´-acetic acid) trithiocarbonate (DDAT) was synthesized according to the method reported by Lai et al.[50] Dicyclohexylcarbodiimide (DCC) and 4-dimethylaminopyridine (DMAP) were purchased from Aldrich. Azobisisobutyronitrile (AIBN) was purchased from Shanghai Chemical Regent Company and recrystallized two

times from ethanol. 4, 4´-Dihydroxybenzophenone (DHBP) and 9,9´-bis (4-hydroxyphenyl) fluorene (BHF) were obtained from Aladdin. 4, 4'-Sulfonylbis (fluorobenzene) (FPS) was purchased from Jiangxi Renming Medicine Medical Industry Company. All other reagents were obtained from Shanghai Chemical Reagent Plant and used as received.

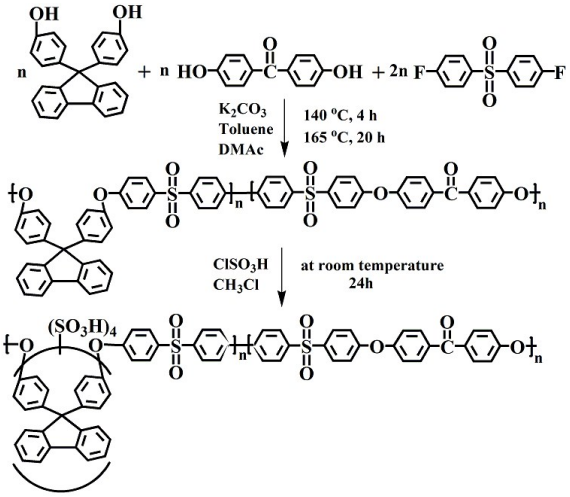

Scheme 2 Synthetic reaction route of SPES.

2.2 Synthesis of sulfonated poly (ether sulfone)

The typical synthetic reaction for sulfonated poly (ether sulfone) is illustrated in Scheme 2. Poly (ether sulfone) was prepared according to the procedure described in the literature.[49] BHF (1.0328 g, 2.947 mmol), DHBP (0.6314 g, 2.947 mmol), FPS (1.4988 g, 5.894 mmol), potassium carbonate (K_2CO_3) (1.635 g), 30 mL N,N-dimethylacetamide (DMAc) and 15 mL toluene were added into three-neck flask equipped with a magnetic stirrer, a Dean-Stark trap and a nitrogen inlet. The reaction was performed under reflux (140 °C) for 4 h under nitrogen protection. Then the temperature of the reaction system was increased to 165 °C and kept for 20 h while the toluene was removed from the system completely. As the reaction proceeded, the viscosity of the solution gradually increased. After the reaction, the system was poured into 500 mL hot ethanol and dried at 70 °C under vacuum for 24 h. ^{1}H-NMR spectrum of PES is shown in Fig. 1. [49] GPC results: M_n = 79900 g mol^{-1}, PDI= 1.54.

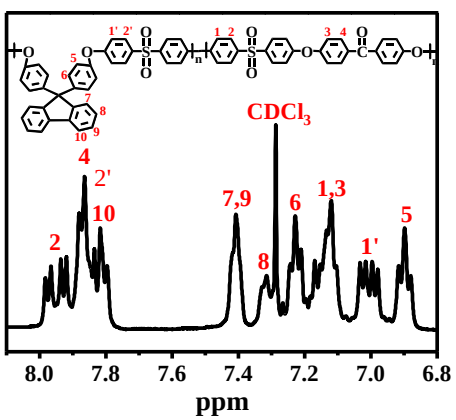

Fig. 1 ^{1}H NMR spectrum of PES using $CDCl_3$ as solvent.

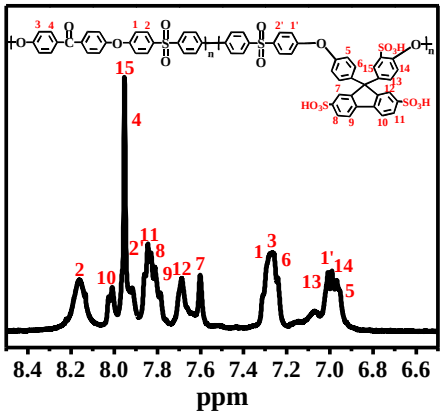

Fig. 2 ^{1}H NMR spectrum of SPES using DMSO-d_6 as solvent.

Poly (ether sulfone) was sulfonated by the following procedure: 0.8 g poly (ether sulfone) and 30 mL chloroform were added into 100 mL three-neck flask. The solution of chlorosulfonic acid (0.7 mL) in chloroform (10 mL) was stirred in a round-bottomed flask, and then the mixed solution was added dropwise to the solution of poly (ether sulfone) in chloroform with a mechanical stirrer. The sulfonation reaction was kept stirring for 24 h until all of the product had precipitated from the reaction mixture. The product was poured into deionized water (500 mL) and filtered, then further washed until the pH is neutral. The final product was dried in a vacuum oven at 70 °C for 12 h. ^{1}H-NMR spectrum of SPES is shown in Fig. 2.[49]

2.3 Preparation of sulfonated polymer brush functionalized graphene oxide (SPB-FGO)

2.3.1 Preparation of GO

GO was synthetized according to the modified Hummers method.[51] Firstly, 1 g graphite powder, 1.25 g $K_2S_2O_8$, 1.25 g P_2O_5 were added into the three round-bottom flask, then 4 mL H_2SO_4 (98%, 4 mL) was added into the flask under the mechanical stirrer at 80 °C for 4.5 h. The solution was cooled to the room temperature and diluted with 170 mL water. The black mixture was filtered using the water pump and washed with water for several times. The black powder was dried at 120 °C in vacuum for 12 h to get the pre-oxidation graphite. Secondly, 1 g pre-oxidation graphite was added into the three round-bottom flask, and 50 mL H_2SO_4 (98%) was slowly added under ice bath to make the solution temperature under 5 °C. Then 5 g $KMnO_4$ was added to the above solution to control the temperature around 20 °C. The color of the solution was dark green. The solution was stirred for 3.5 h at 35 °C in water bath, and 30 mL water was added slowly into the above solution and the temperature was controlled under 50 °C. Then the mixture was stirred for another 15 min at 98 °C and the color of the solution turned into bright yellow. The resulting mixture was diluted with additional 240 mL of water and followed by adding 6 mL of 30 wt % H_2O_2. The resulting mixture was centrifuged and washed with 10 wt % HCl solution several times. After that, the mixture was washed with water completely to remove the residual acid. Finally, the graphite oxide dispersion (0.1 mg mL^{-1}) was exfoliated by water bath and ultrasounded (300 W) for 1 h. GO dispersion was obtained by high speed centrifugation and dried

by freeze-drying.

2.3.2 Synthesis of A-GO

A-GO was prepared according to the previous reports.[52,53] 21 mg GO was dispersed into 21 mL H_2O by ultrasonication for 1 h to get a homogeneous GO dispersion and then 5.2 mL APTES was added to the solution by ultrasonication for another 1 h. Finally, the mixture was poured into a three-neck flask to react for 8 h at 60 ^oC under nitrogen atmosphere. The suspension was filtered and washed thoroughly with ethanol and water, respectively, and at last dried in a vacuum oven overnight.

2.3.3 Preparation of SPB-FGO

In a typical reaction for preparation of RAFT agent functionalized GO (A-FGO), 0.1 g A-GO, 0.73 g DDAT, 0.12 g DMAP and 50 mL N,N-dimethylformamide (DMF) were added into 100 mL round-bottom flask by ultrasonication for 30 min to guarantee the solution dispersed completely, after that the mixture was stirred in the ice-water bath for 1 h. 0.41 g DCC was added and the reaction was kept for 48 h at room temperature. The reaction mixture was vacuum-filtered through a polycarbonate film (Φ = 0.22 μm), and the collected product (A-FGO) was washed with ethanol, deionized water and tetrahydrofuran (THF), respectively, to remove the unreacted DDAT. The following RAFT polymerization for grafting polymer brush from GO was carried out according to the modified procedure:[54] SS (1.0 g), A-FGO (0.1 g), AIBN (1.0 mg) and DMF (6 mL) was stirred in an oil bath of 60 ^oC for 12 h. Finally, the product was washed with DMF three times to remove the untreated SS and the product was collected by centrifugation, then the product was dried in vacuum oven overnight. The above product was immersed into the 1 M HCl solution, and then the final product was collected by centrifugation with water until the solution was close to neutral.

2.4 Preparation of composite membranes

The composite membranes were prepared via a simple solution casting method and the preparation process was as follows : 0.6 g SPES was dissolved in 8 mL DMF under magnetic stirrer at 70 ^oC until SPES dissolved completely, and then a certain amount of SPB-FGO was ultrasonicated in 2 mL DMF to obtain a homogeneous black dispersion. The above SPB-FGO dispersion was mixed with the SPES solution and kept stirring for 6 h at 70 ^oC. The mixture solution was degassed with water pump, then was cast onto a glass dish and dried at 60 ^oC for another 6 h, finally heated at 120 ^oC for 12 h in a vacuum oven to obtain the membranes. The thicknesses of all dry membranes were measured to be 30-50 μm.

2.5 Measurements

2.5.1 Instrumental characterizations

Fourier transform infrared (FTIR) spectra were recorded on a Magna 560 FTIR spectrometer. Thermogravimetric analysis (TGA) was conducted utilizing a Perkin-Elmer TGA-2 thermogravimetric analyzer by heating the samples from ambient temperature to 800 ^oC with a heating rate of 10 ^oC min^{-1} in nitrogen. The morphologies of fractured surfaces of membranes obtained by brittle breakage using liquid nitrogen were studied using scanning electron microscopy (SEM) (XL-30 ESEM FEG, FEI Company). The morphology characterization was carried out using a JEM-2100F transmission electron microscope (TEM). The membranes were stained with silver ions by immersing in 0.5 M $AgNO_3$ aqueous solution overnight. The molecular weight of PES was measured at a flow rate of 1.0 mL min^{-1} at 40 ^oC by gel permeation chromatography (GPC) equipped with Waters 515 HPLC Pump and Waters 2414 differential refractive index detector. DMF containing 0.05 M LiBr was used as eluent, and the molecular weights were determined vs polystyrene standards. ^{1}H-NMR spectra were recorded on a Bruker Avance 500 MHz NMR using deuteroxide (D_2O), deuterochloroform ($CDCl_3$) or deutrated dimethyl sulfoxide (DMSO-d_6) as the solvent. Gas chromatography (GC) was carried out on an SP-3400 AGILENT 6890, and the analytes were separated on a 30 m × 0.32 mm DB-Wax (0.25 μm film thickness) capillary column, using nitrogen at a constant flow of 2 mL min^{-1} as carrier gas. The column temperature was 60 ^oC, both the injector and DET (FID) temperature were 200 ^oC. The X-ray photoelectron spectroscopy (XPS) spectra were obtained from the surfaces with a diameter of 500 μm in area by means of a Quantum 2000 spectrometer using a non-monochromatized Al K_α excitation radiation. The tensile measurements were performed on an Instron Model 1122 (F S=20N) at 25 ^oC with the tensile rate of 5 mm min^{-1} at 50 % relative humidity.

2.5.2 Water uptake and swelling ratio

The membranes were dried in a vacuum oven at 80 ^oC for 12 h and weighed, then the membranes were immersed into deionized water for more than 24 h and weighed. The water uptake could be calculated by the following equation:

$$\text{Water uptake (WU)} = [(W_{wet} - W_{dry})/W_{dry}] \times 100\% \quad (1)$$

where W_{wet} is the weight of wet membrane and W_{dry} is the weight of dried membrane.

The swelling ratio of the membranes was calculated by immersing the membranes in deionized water at room temperature for 24 h, the changes in length (ΔL) and thickness (ΔT) were calculated by the following equation:

$$\Delta L = [(L-L_S)/L_S] \times 100\%; \quad \Delta T = [(T-T_S)/T_S] \times 100\% \quad (2)$$

where L (cm) is the length of wet membrane and L_S (cm) is the length of dried membrane; T (μm) is the thickness of wet membrane and T_S (μm) is the thickness of dried membrane.

2.5.3 Ion-exchange capacity (IEC)

The ion-exchange capacity (mmol of sulfonic acid g^{-1} of sample) of membrane was measured by back-titration. The membranes were immersed in 2 M NaCl solution for 48 h to exchang the H^+ for Na^+, and then the exchanged H^+ was titrated with 0.01 M NaOH using phenlphthalein as the indicator. IEC values of the membranes were calculated by the following equation:

$$IEC = (V_{NaOH} \times C_{NaOH})/W_{dry} \text{ (mmol } g^{-1}) \quad (3)$$

where W_{dry} (g) is the weight of dried membrane, V_{NaOH} (L) is the titrated volume of NaOH solution, and C_{NaOH} (mol L^{-1}) is the concentration of NaOH solution.

2.5.4 Proton conductivity

Proton conductivity was measured by the AC impedance method using an electrochemical work station. The membranes were immersed in deionized water for 24 h to make the membranes full hydration. Then cut the membranes into the rectangle of 4 cm ×1 cm. The conductivity of the composite membrane was measured using a modified four-probe AC impedance method

over the frequency range 1 Hz-100 kHz. Through the measurement of electrochemical work station, the resistance of each membrane could be obtained. The proton conductivity (σ) was calculated by the following equation:

$$\sigma = L/RA \quad (4)$$

where σ (S cm^{-1}) is the proton conductivity, L (cm) is the distance between the two electrodes, A (cm^2) is the cross-sectional area of the membrane and R (Ω) is the resistance of the membrane.

2.5.5 Methanol permeability

Methanol permeability was measured using a liquid permeation cell as described in the literature.[55] The membrane sample was sandwiched between the two cells, where one side was 8 M methanol solution, and the other side was deionized water. The permeation cell was continuously stirred during the experiment. The concentration of methanol in the deionized water side was measured by gas chromatography (GC). Methanol permeability was calculated by the following equation:

$$C_B(t) = APC_A(t - t_0)/V_BL \quad (5)$$

where A (cm^2) is the diffusion area, V_B (cm^3) is the volume of permeated reservoirs, and L (cm) is the thickness of the membrane. C_A and C_B (mol L^{-1}) are the methanol concentration of the two sides. P (cm^2 s^{-1}) is methanol permeability and $t-t_0$ (s) is the time of methanol permeability.

2.5.6 Oxidative stability

Oxidative stability was measured by immersing a small piece of membrane sample with a size of about 1 × 1 cm^2 in Fenton's reagent (30 ppm $FeSO_4$ in 30 wt % H_2O_2) at room temperature. The stability was evaluated by recording the time when membranes began to dissolve (τ1) and dissolve completely (τ2).

3. Results and discussion

3.1 Characterization of SPB-FGO

The preparation of SPB-FGO could be divided into four steps as illustrated in Scheme 1. The first step is the hydrolysis and condensation reaction between the alkoxylsilane groups of APTES and the hydroxyl groups on the surface of GO to obtain A-GO. The second step is the amidation reaction between amino groups of A-GO and carboxyl groups of DDAT to obtain A-FGO. The third step is the AIBN initiated RAFT polymerization reaction of SS from the surface of A-FGO. The last is the exchange of Na^+ with H^+ to obtain the sulfonated polymer brush functionalized GO (SPB-FGO).

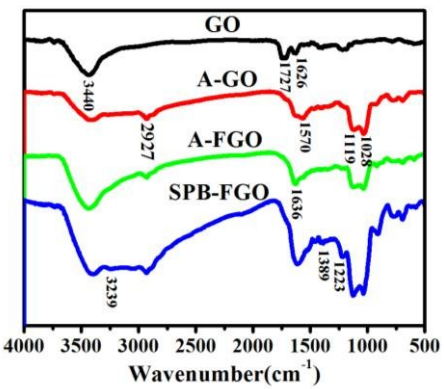

Fig. 3 FT-IR spectra of GO, A-GO, A-FGO and SPB-FGO.

The FT-IR spectra of GO, A-GO, A-FGO and SPB-FGO are shown in Fig. 3. For the FT-IR spectrum of GO, the characteristic absorption peak at 3440 cm^{-1} is from –OH stretching vibration, and the peak at 1727 cm^{-1} is ascribed to C=O stretching vibration. The peak at 1626 cm^{-1} is due to ether/epoxy stretching vibration. The existence of these characteristic peaks indicates that the graphite has been successfully oxidized. For the A-GO, some new absorption peaks appear. The absorption band at 2927 cm^{-1} is the -CH_2 stretching vibration of APTES in A-GO. The broad absorption peak at 1570 cm^{-1} is corresponding to the -NH_2.[56] The stretching vibration band at 1119 cm^{-1} is due to Si-C and the stretching vibration band at 1028 cm^{-1} is attributed to Si-O-Si.[56] As for A-FGO, the new absorption peak at 1636 cm^{-1} is attributed to the amide band between the amino group of APTES and the carboxyl group via the amidation reaction.[57] As for SPB-FGO, there are some new absorption peaks due to the introduction of SS units. The absorption band at 3239 cm^{-1} is attributed to the benzene ring, and the characteristic bands of sulfonic acid groups are at 1389 and 1223 cm^{-1}.[54]

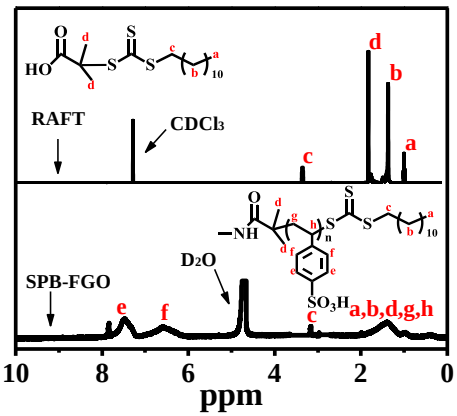

Fig. 4 ^{1}H NMR spectra of RAFT and SPB-FGO.

Fig. 4 is the ^{1}H NMR spectra of RAFT and SPB-FGO. For SPB-FGO, it can be seen that there are three broad peaks. The peaks at 6.56 and 7.45 ppm are corresponding to the hydrogen of benzene ring. The peak at 1.36 ppm is ascribed to the hydrogen of -CH, -CH_2, -CH_3.[58] These results demonstrate that PSS brushes have been grafted onto the surface of GO successfully. In the ^{1}H NMR spectra of RAFT and SPB-FGO, the peak c represents the hydrogen on -CH_2-. The peaks (e+f) represent the hydrogen on benzene ring. The area integral ratio of c and (e+f) of hydrogen is 1:50, and the degree of polymerization (*n*) can be calculated as 25. Therefore, the number-average molecular weight (M_n) of PSS on GO can be calculated to be 4600 g mol^{-1}.

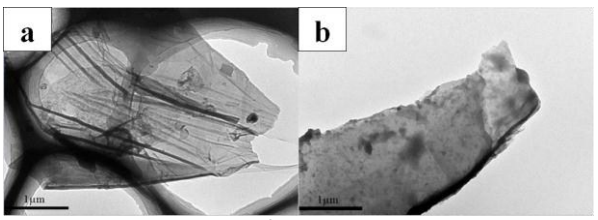

Fig. 5 TEM images of GO (a) and SPB-FGO (b).

The morphologies of GO and SPB-FGO were measured by TEM and the results are shown in Fig. 5. GO is a sheet with some

wrinkles, which is probably caused by GO agglomeration because of the strong interlayer attractions. With the sulfonated polymer brush coated onto the surface of GO, the thickness of the sheet became thicker, which was caused by the presence of sulfonic acid-containing polymer brushes that weakened the interlayer interactions of SPB-FGO.[59]

X-ray photoelectron spectroscopy (XPS) was employed to further explore the chemical structure of modified GO. Fig.6 shows the XPS spectra of A-FGO and SPB-FGO samples, and the mass fractions of different atoms are listed in Table 1. For A-FGO, a peak at 163.5 eV corresponding to the binding energy of S element of trithiocarbonate is observed and the weight percentage of S atom is 3.68 %.[57] However, for SPB-FGO, there is a new peak at 167.9 eV corresponding to the binding energy of $-SO_3H$ of SPB-FGO, and the weight percentage of S atom is 6.69 %.[60] The above results demonstrate that PSS has been successfully grafted onto the surface of GO.

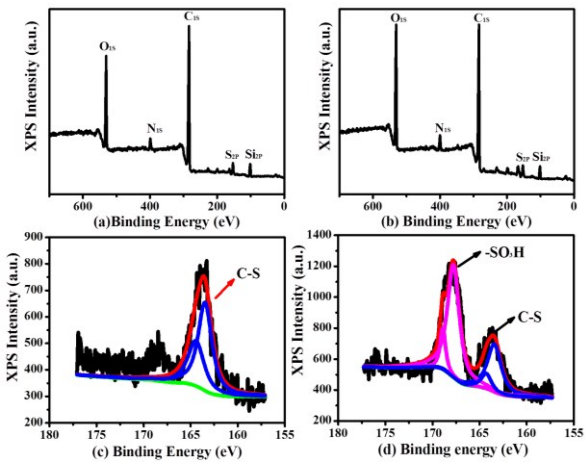

Fig. 6 XPS spectra of A-FGO (a, c) and SPB-FGO (b, d).

Table 1 Mass fractions of different atoms for A-FGO and SPB-FGO

Samples	Atomic composition (wt %)				
	C	N	Si	S	O
A-FGO	59.76	3.72	13.54	3.68	19.30
SPB-FGO	53.23	4.54	11.82	6.69	23.72

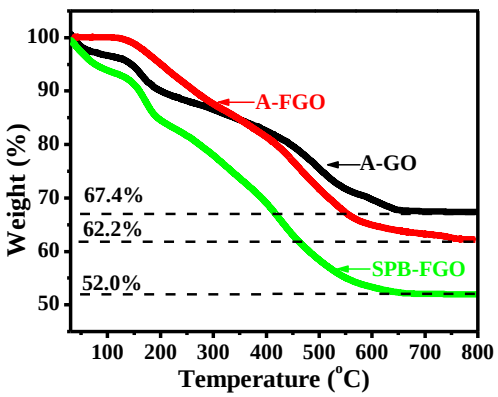

Fig. 7 TGA curves of A-GO, A-FGO and SPB-FGO.

The evidence for the thermal stability and the grafting degree of RAFT agent and PSS on GO sheet can be obtained from TGA as shown in Fig. 7. It can be seen that the three samples (A-GO, A-FGO, SPB-FGO) display three-stage weight losses, including the bonded water as the first stage (50-200 °C), the degradation of the oxygen functional groups as the second stage (210-400 °C) and the decomposition of GO backbone as the third stage (410-800 °C). For the first stage, the SPB-FGO has a higher weight loss, because the existence of $-SO_3H$ groups improves the water absorption ability. For the second stage, the weight losses of A-GO and A-FGO are caused by the decomposition of oxygen functional groups and the weight loss of SPB-FGO is caused by the pyrolysis of sulfonic acid groups. For the third stage, SPB-FGO exhibits the higher weight loss, indicating that the loading amount of $-SO_3H$ is higher and the polymer brush length is longer.[22] For the modified GO samples (A-GO, A-FGO and SPB-FGO), the residues at 800 °C are higher than that of usual GO and its organic-modified materials. This is because the alkoxylsilane (APTES) grafted GO (A-GO) containing Si-O-Si bond could convert to stable inorganic silica at high temperature.

It is an important challenge in the present synthetic strategy for the control of grafting density of the polymer brushes on particle surface. The grafting density can be measured from the formula according to TGA analysis as follow:[32]

Functional groups per carbon: $\tilde{A}_{mg} = M_C \times W_F / M_F \times W_C$

Where M_C is the relative molar mass of carbon (M_C = 12 g mol^{-1}), M_F is the molecular weight of functionalized groups (RAFT agent: M_F= 364 g mol^{-1}), and W_C and W_F are the weight fractions of A-GO backbone and the functionalized groups, respectively. W_C (W_C= 67.4 %) and W_F (W_F= 32.6 %) can be readily obtained from the TGA curves of the functionalized groups. Then it can be calculated that the grafting density of RAFT agent on A-GO sheets is 1.59 functional groups per 100 carbons.

Chain per carbon : $\tilde{A}_{pg} = M_C \times W_P / M_P \times W_C$

where M_C is the relative molar mass of carbon (M_C = 12 g mol^{-1}), M_P is the average molecular weight (M_n) of grafted polymer, and W_C and W_P are the weight fractions of the polymer–graphene backbone (not including RAFT agent groups and grafted polymer) and the grafted polymer, respectively. W_C (W_C = 52 %) and W_P (W_P = 48 %) can be readily obtained from the TGA curves of SPB-FGO composites. So, the grafting density of PSS chains on GO sheets can be calculated to be 0.24 chains per 100 carbons.

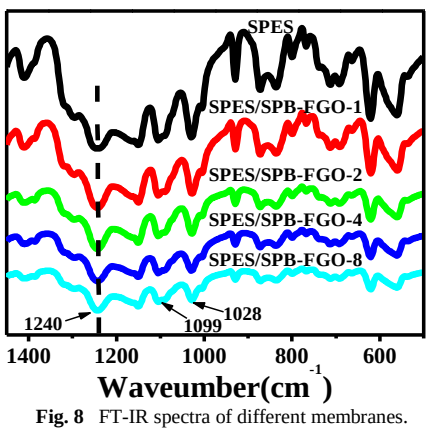

Fig. 8 FT-IR spectra of different membranes.

3.2 Characterization of polymer composite membranes

3.2.1 FT-IR and microstructure of composite membranes.

Fig. 8 shows the FI-IR spectra of SPES and its composite membranes with different loading weights of SPB-FGO. All the

composite membranes exhibit three characteristic absorption peaks at 1240, 1099 and 1028 cm^{-1} of sulfonic groups assigned to S=O stretching, symmetric and asymmetric stretching vibration of O=S=O, respectively.[22] For the composite membranes, no new bands are observed, including that no chemical bands are formed between the fillers and SPES matrix. Compared with the composite membranes, the band intensity of pristine SPES membrane is the highest. When the content of fillers increases, the band intensity of composite membrane is gradually weakened. The above phenomenon can be explained by the electrostatic interactions between SPES matrix and inorganic fillers, and the similar observations were found in other composite membranes.[13,61]

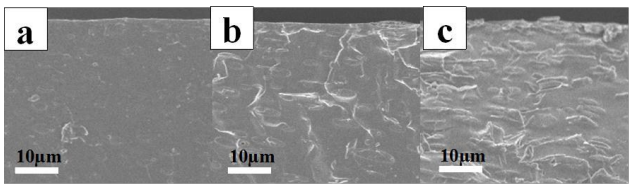

Fig. 9 SEM images of SPES (a), SPES/SPB-FGO-2 (b) and SPES/SPB-FGO-8 (c).

Fig. 9 is the SEM images of SPES, SPES/SPB-FGO-2 and SPES/SPB-FGO-8 composite membranes. The cross-section of the different membranes was obtained by brittle breakage in liquid nitrogen. The cross-section of the pristine SPES membrane exhibits a smooth surface without any cracks, indicating the fine performance of the membrane. The cross-section of the composite membranes becomes rougher and the roughness increases with the increasing content of fillers. There is no obvious phase separation in all the composite membranes because both SPES matrix and SPB-FGO have the same sulfonic acid groups, which can provide better compatibility between the matrix and the doped fillers, and the fillers of SPB-FGO exhibit uniform distribution in the SPES matrix as a result of the good interfacial interactions between SPB-FGO and SPES matrix.[22]

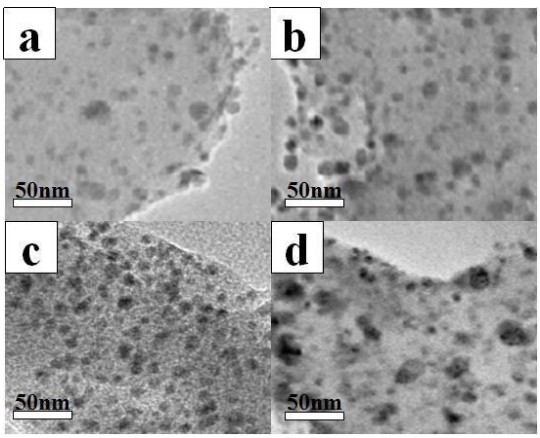

Fig. 10 TEM images of SPES (a), SPES/SPB-FGO-1 (b), SPES/SPB-FGO-2 (c) and SPES/SPB-FGO-8 (d).

The microstructure of the pristine SPES membrane and composite membranes were studied by TEM. The membranes are stained with silver ions by immersing in 0.5 M $AgNO_3$ aqueous solution overnight. As shown in Fig.10, the dark spherical regions are hydrophilic domains, and there are sulfonic acid ion clusters in these regions, while the white regions are attributed to the hydrophibic domains. As can be seen from TEM image in Fig. 10c for SPES/SPB-FGO-2, the ion clusters are well-distributed and their sizes are more uniform. The reason can be interpreted as followed: the strong interfacial interactions between SPB-FGO and SPES can reduce the size of ion clusters and prevent the ion clusters from aggregating. Moreover, the small ion clusters can shorten the distance between the ion clusters, which can decrease the barrier for the proton to hop from one cluster to the next.[62,63] For other TEM images, the ion clusters are not well-distributed and some aggregations can be observed in Fig.10d, which may block the proton transfer channels.[61]

Table 2 Mechanical properties and oxidative stability of different membranes

Samples	Young's modulus (MPa)	Tensile strength (MPa)	Elongation at break (%)	Oxidative stability[b] (h)	
				$\tau1$[c]	$\tau2$[d]
SPES	1367	44.1	6.8	3.3	5.0
SPES/SPB-FGO-1	1860	51.5	5.3	3.5	5.3
SPES/SPB-FGO-2	2070	52.2	4.4	3.9	5.8
SPES/SPB-FGO-4	2120	52.3	3.5	4.3	7.0
SPES/SPB-FGO-8	2150	54.4	3.0	4.6	7.5
Nafion117[a]	357	30.3	270	-	-

[a] The value was measured at the same condition with composite membranes.
[b] Measured at room temperature in 30 wt% H_2O_2 containing 30 ppm $FeSO_4$.
[c] The time when the membrane broke into pieces.
[d] The time when the membrane dissolved completely.

3.2.2 Mechanical properties and thermogravimetric analysis.

The mechanical properties of the pristine SPES membrane and composite membranes were measured at room temperature and 50 % relative humidity, and the results are listed in Table 2. Both the Young's modulus and the tensile strength of the composite membranes are higher than that of the pristine membrane and Nafion membrane.[64] The elongations at break of the composite membranes are lower than that of the pristine membrane and Nafion membrane. As a whole, the mechanical properties of the composite membranes are better than that of the pristine membrane and Nafion membrane, which is in accordance with that reported in previous studies.[65,66] This result is mainly due to the mechanical reinforcement by the inorganic fillers and the interfacial adhesion or strong hydrogen bonds between SPB-FGO and SPES matrix. Moreover, the well dispersion of SPB-FGO in the SPES matrix can promote the efficient load transfer between the matrix and SPB-FGO fillers, and simultaneously reduce the stress convergence during the elongation process.[56] The mechanical properties of the pristine SPES and SPES/SPB-FGO composites membranes are higher than those of the sulfonated GO modified SPEEK based composite membranes that reported in previous studies.[22,61] The above results indicate that the SPES/SPB-FGO membranes are suited to be used as PEMs.

The thermal stability of the membranes for fuel cell is very important. As shown in the TGA curves (Fig. 11), the thermal decomposition of the membranes can be divided into three main stages. The initial weight loss from 30-100 ^oC is induced by the evaporation of absorbed water or residual solvent in membranes. The second weight loss is from 280-390 ^oC, which is corresponding to the decomposition of sulfonic acid groups of

different membranes. The third weight loss around 500 °C is caused by the decomposition of the SPES main chains.[11] The pristine membrane and composite membranes exhibit almost the same degradation trends. All the membranes have the good thermal stability.

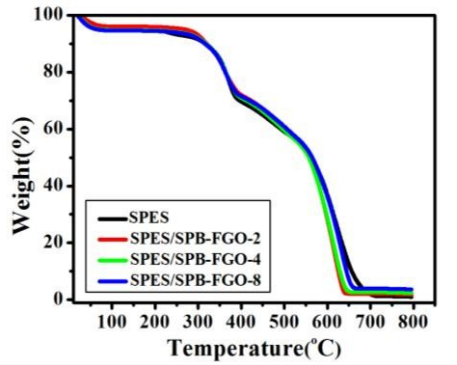

Fig. 11 TGA curves of different membranes.

3.2.3 IEC, water uptake and swelling ratio.

IEC, water uptake (WU) and swelling ratio values of the pristine membrane and composite membranes are shown in Table 3. The IEC value is an indication of the concentration of sulfonic acid groups in proton exchange membranes. As shown in Table 3, the IEC, WU and swelling ratio values have the same tendency. When the content of inorganic fillers is increased to 2 wt%, all the three values reach the maximum. The above results demonstrate that the IEC, WU and swelling ratio values of the composite membranes all increase with the increasing concentration of hydrophilic sulfonic acid groups. When the inorganic fillers exceed 2 wt %, the IEC, WU and swelling ratio all begin to drop. The reduction of the IEC is probably caused by the aggregation of the fillers when the content of fillers is higher, which may result in a lower IEC value of SPB-FGO as compared with that of the SPES matrix. Both the water uptake and swelling ratio have the same tendency, indicating that the increase of the inorganic fillers may lead to the aggregation in SPES matrix, thus blocks the water molecules to enter.[67]

3.2.4 Proton conductivity, methanol permeability and selectivity.

The proton conductivity of the membranes plays an important role in fuel cell performance. The proton conductivities of the pristine membrane and composite membranes are shown in Fig. 12. The proton conductivity of the pristine membrane is 0.0155 S cm^{-1} at 25 °C. When the content of the fillers is 2 wt%, the proton conductivity reaches the maximum value of 0.0289 S cm^{-1}. These results demonstrate that the incorporation of SPB-FGO into SPES matrix can serve as wider pathways for proton transfer to get higher proton conductivity.[28] Compared with other reported proton conductivities of SPEEK based composite membranes with GO or sulfonated GO,[22,61,68] Both the SPES matrix and SPES/SPB-FGO membranes in this work exhibit higher proton conductivity. With the increase of temperature, the conductivities of the membranes are all improved. The above results demonstrate that the high temperature can promote the proton transfer in polymer matrix because the hopping or the diffusion of proton becomes faster under this condition based on the vehicle mechanism and the Grotthus (hopping) mechanism.[69] Typically, the proton conductivity is affected by water uptake and the microstructure of the membranes.

Generally, the water uptake can affect the Vehicle mechanism and Grotthuss mechanism. So, for the vehicle mechanism, the protons in the SPES/SPB-FGO composite membranes with higher water uptake can combine with unprotonated vehicles (H_2O) and protonated vehicles (H_3O^+) diffuse as a whole across the membrane forming a net to facilitate the transportation of protons.[70] And for the Grotthuss mechanism, the membranes with higher water uptake can lead to the proton diffuses through the hydrogen bond network of water molecules.[11] Because SPB-FGO has a high surface area with a large amount of sulfonic acid groups, the composite membranes can hold more water and consequently can facilitate the transfer of more protons to get higher proton conductivity. As shown in Table 3, the water uptake of the pristine membrane is 19.7 % and the proton conductivity of the pristine membrane is 0.0155 S cm^{-1}. Compared with the pristine membrane, the values of water uptake and proton conductivity of the SPES/SPB-FGO-2 increase by 29 % and 86 %, respectively. Therefore, the higher water uptake can lead to the higher proton conductivity. In addition, from the above microstructure of the membranes (see Fig.10) can be seen that the SPB-FGO-2 sheets are well-distributed in the SPES matrix with the small ion clusters. The well-distributed hydrophilic sulfonic acid ion clusters can increase the proton conductivity. Therefore, the composite membrane with 2 wt% SPB-FGO at 80 °C shows the highest proton conductivity of 0.0852 S cm^{-1}. As shown in Fig. 12, when the loading content of the fillers exceeds 4 wt%, the proton conductivity begins to reduce. This result should be partially contributed to the "block effect" caused by the aggregation of inorganic fillers in the polymer matrix. The "block effect" could reduce the number of the proton transfer channels. As a consequence, the conductivity of the composite membranes begins to decrease. So, the appropriate amount of SPB-FGO has better effect on the improvement of proton conductivity.

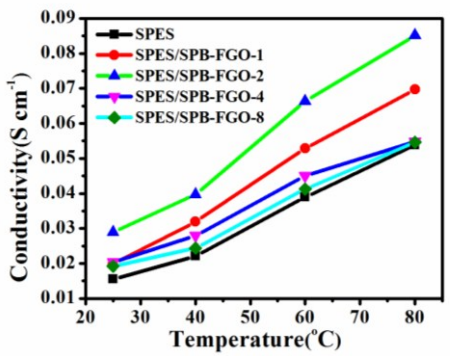

Fig. 12 Proton conductivities of different membranes at 25, 40, 60 and 80 °C.

Methanol permeability also is an important property for PEMs. The different methanol permeability values of the pristine membrane and composite membranes are shown in Table 3. With the increasing loading content of the fillers, the methanol permeability is gradually reduced. The methanol permeability of pristine membrane is 9.3×10^{-7} cm^2 S^{-1}, while that of the composite membrane with 8 wt% of SPB-FGO is reduced to

6.9×10^{-7} cm^2 S^{-1}. The above results illustrate that the interaction between SPB-FGO and SPES can shorten the ion clusters in size and restrict the formation of the methanol transfer channels, therefore lead to the reduction of methanol permeability.[67,71] The selectivity values of the pristine membrane and composite membranes are also listed in Table 3. The selectivity of the pristine membrane is 1.7×10^4 S s cm^{-3}, while the selectivities (2.4×10^4~3.5×10^4 S s cm^{-3}) of the composite membranes are all higher than that of the pristine membrane. The high proton conductivity and the low methanol permeability of SPES/SPB-FGO-2 composite membrane make it suitable for the fuel cells.

Table 3 IEC, WU, Swelling ratio, proton conductivity, methanol permeability and selectivity

Samples	IEC (mmol g^{-1})	WU (%)	Swellig ratio (%)		σ (S cm^{-1})		P_M (10^{-7}cm^2 S^{-1})	Selectivity (10^4S s cm^{-3})
			ΔT	ΔL	25°C	80 °C		
SPES	1.40	19.7	11.4	18.1	0.0155	0.0539	9.3	1.7
SPES/SPB-FGO-1	1.47	23.5	16.7	18.7	0.0198	0.0697	8.3	2.4
SPES/SPB-FGO-2	1.52	25.5	20.0	21.6	0.0289	0.0852	8.2	3.5
SPES/SPB-FGO-4	1.43	23.3	15.1	18.5	0.0203	0.0548	8.1	2.5
SPES/SPB-FGO-8	1.42	22.8	12.9	18.2	0.0192	0.0546	6.9	2.8

3.2.5 Oxidative stability.

The oxidative stabilities of the SPES and SPES/SPB-FGO membranes were measured by immersing the samples into the Fenton's reagent (30 ppm $FeSO_4$ in 30 wt % H_2O_2) at room temperature. The stability was investigated by measuring the elapsed time when the membrane began to break into pieces (τ1) and the time when the membrane dissolved completely (τ2).[72] As shown in Table 3, with the increasing loading content of the fillers, the two values both increase and are higher than that of the pristine membrane. The above results illustrate that the hydrophilic SPB-FGO sheets seem to be somewhat effective in increasing the tolerance of a radical attack independent of SPB-FGO particle dispersion. In particular, the SPB-FGO sheets with small size and high surface area might help the composite membranes to enhance the oxidative radical stability.[73]

4. Conclusions

Sulfonated polymer brush functionalized graphene oxide (SPB-FGO) was prepared via the RAFT polymerization, and then was introduced into SPES matrix to prepare a series of composite proton exchange membranes. The SPES/SPB-FGO composite membranes had the following advantages: (I) SPES matrix showed better mechanical property, thermal stability and higher proton conductivity; (II) through "grafting from" method based on RAFT polymerization, the polymer chains could grow from the modified GO sheets to achieve excellent control over the grafting density; (III) connecting the ionic clusters in SPES via the sulfonic acid groups on SPB-FGO; (IV) generating wide and continuous proton conducting pathways via the sulfonated polymer brushes on PB-FGO surface. When the loading content of the fillers was 2 wt%, the proton conductivity reached the maximum of 0.0289 S cm^{-1}. However, the proton conductivity began to reduce due to the "block effect" when the loading content of the fillers was above 4 wt%. With the increasing loading content of SPB-FGO, the composite membranes showed higher water uptake, better mechanical property, thermal stability and lower methanol permeability. In generally, the comprehensive performances of the composite membranes were better than the pristine membrane. Summarily, the SPB-FGO polymer brush modified composite membranes could be considered as a promising candidate material for PEMs.

Acknowledgments

We would like to appreciate the financial support of the National Natural Science Foundation of China (2157040044).

Notes and references

[a] *Institute of Chemistry, Northeast Normal University, Changchun 130024, PR. China.*
** Address correspondence to: lucl055@nenu.edu.cn.*
[b] *College of Life Sciences, Jilin Agricultural University, Changchun 130118, P. R. China*

1 L. Fu, G. Xiao and D. Yan, *J. Mater. Chem*., 2012, **22**, 13714.
2 Q. He, J. Zheng and S. Zhang, *J. Power Sources*, 2014, **260**, 317.
3 J. Rozière and D. J. Jones, *Annu. Rev. Mater. Res*., 2003, **33**, 503.
4 X. Zhang, L. Sheng, T. Higashihara and M. Ueda, *Polym. Chem.*, 2013, **4**, 1235.
5 X. Zhang, Z. Hu, L. Luo, S. Chen, J. Liu, S. Chen and L. Wang, *Macromol Rapid commun.*, 2011, **32**, 1108.
6 K. Si, D. Dong, R. Wycisk and M. Litt, *J. Mater Chem.*, 2012, **22**, 20907.
7 X. Zhang, S. Chen, J. Liu, Z. Hu, S. Chen and L. Wang, *J. Membr Sci.*, 2011, **371**, 276.
8 N. Zhang, B. Wang, C. Zhao, Y. Zhang, F. Bu, Y. Cui, X. Li and H. Na, *J. Power Sources*, 2015, **275**, 815.
9 J. Ma, H. -J. Ni, D. -Y. Su, M. -Y. Huang and X. -X. Wang, *Int. J. Hydrog. Energy*, 2012, **37**, 13185.
10 E. Bakangura, L. Ge, M. Muhammad, J. Pan, L. Wu and T. Xu, *J. Membr. Sci*., 2015, **475**, 30.
11 Y. He, C. Tong, L. Geng, L. Liu and C. Lü, *J. Membr Sci.*, 2014, **458**, 36.
12 Y. Choi, Y. Kim, H. K. Kim and J. S. Lee, *J. Membr Sci.*, 2010, **357**, 199.
13 T. Xu, W. Hou, X. Shen, H. Wu, X. Li, J. Wang and Z. Jiang, *J. Power Sources*, 2011, **196**, 4934.
14 F. Beckert, C. Friedrich, R. Thomann and R. Mülhaupt, *Macromolecules*, 2012, **45**, 7083.
15 B. G. Choi, Y. S. Huh, Y. C. Park, D. H. Jung, W. H. Hong and H. Park, *Carbon*, 2012, **50**, 5395.
16 L. Wang, A. Lai, C. Lin, Q. Zhang, A. Zhu and Q. Liu, *J. Membr Sci.*, 2015, **492**, 58.
17 D. R. Dreyer, S. Park, C. W. Bielawski and R. S. Ruoff, *Chem Soc Rev.*, 2010, **39**, 228.
18 L. J. Cote, F. Kim and J. Huang, *J. Am. Chem. Soc.*, 2009, **131**, 1043.
19 H. J. Salavagione, G. Martinez and G. Ellis, *Macromol. Rapid commun*., 2011, **32**, 1771.
20 B. G. Choi, J. Hong, Y. C. Park, D. H. Jung, W. H. Hong, P. T. Hammond and H. Park, *ACS Nano*, 2011, **5**, 5167.
21 K. Feng, B. Tang and P. Wu, *J. Mater. Chem A*., 2014, **2**, 16083.
22 L. Zhao, Y. Li, H. Zhang, W. Wu, J. Liu and J. Wang, *J. Power*

Sources, 2015, **286**, 445.
23 P. P. Sharma and V. Kulshrestha, *RSC. Adv*., 2015, **5**, 56498.
24 Y. Zhao, Z. Jiang, D. Lin, A. Dong, Z. Li and H. Wu, *J. Power Sources*, 2013, **224**, 28.
25 H. Pan, Y. Zhang, H. Pu and Z. Chang, *J. Power Sources*, 2014, **263**, 195.
26 Y. Liu, J. Wang, H. Zhang, C. Ma, J. Liu, S. Cao and X. Zhang, *J. Power Sources*, 2014, **269**, 898.
27 G. He, Y. Li, Z. Li, L. Nie, H Wu, X. Yang, Y. Zhao and Z. Jiang, *J. Power Sources*, 2014, **248**, 951.
28 H. Bai, H. Zhang, Y. He, J. Liu, B. Zhang and J. Wang, *J. Membr Sci.*, 2014, **454**, 220.
29 Y. Li, G. He, S. Wang, S. Yu, F. Pan, H. Wu and Z. Jiang, *J. Mater. Chem. A.*, 2013, **1**, 10058.
30 X. Chen, L. Yuan, P. Yang, J. Hu and D. Yang, *J. Polym. Sci. Part A: Polym. Chem.*, 2011, **49**, 4977.
31 A. Badri, M. R. Whittaker and P. B. Zetterlund, *J. Polym. Sci., Part A: Polym. Chem*., 2012, **50**, 2981.
32 Y. S. Ye, Y. N. Chen, J. S. Wang, J. Rick, Y. J. Huang, F. C. Chang and B. J. Hwang, *Chem. Mater.*, 2012, **24**, 2987.
33 K. Ohno, T. Morinaga, K. Koh, Y. Tsujii and T. Fukuda, *Macromolecules*, 2005, **38**, 2137.
34 S. H. Lee, D. R. Dreyer, J. An, A. Velamakanni, R. D. Piner, S. Park, Y. Zhu, S. O. Kim, C. W. Bielawski and R. S. Ruoff, *Macromol. Rapid commun.*, 2010, **31**, 281.
35 G. Pan, Y. Ma, Y. Zhang, X. Guo, C. Li and H. Zhang, *Soft Matter*, 2011, **7**, 8428.
36 K. Ohno, Y. Ma, Y. Huang, C. Mori, Y. Yahata, Y. Tsujii, T. Maschmeyer, J. Moraes and S. Perrier, *Macromolecules*, 2011, **44**, 8944.
37 J. Yan, C. Liu, Z. Wang, W. Xing and M. Ding, *Polymer*, 2007, **48**, 6210.
38 H. Wei, G. Chen, L. Cao, Q. Zhang, Q. Yan and X. Fang, *J. Mater. Chem. A.*, 2013, **1**, 10412.
39 F. Gong and S. Zhang, *J. Power Sources*, 2011, **196**, 9876.
40 B. P. Tripathi, T. Chakrabarty and V. K. Shahi, *J. Mater. Chem.*, 2010, **20**, 8036.
41 K. T. Park, J. H. Chun, S. G. Kim, B. -H. Chun and S. H. Kim, *Int. J. Hydrog. Energy*, 2011, **36**, 1813.
42 Z. Bai, G. E. Price, M. Yoonessi, S. B. Juhl, M. F. Durstock and T. D. Dang, *J. Membr Sci.*, 2007, **305**, 69.
43 G. Wang, G. Xiao and D. Yan, *J. Membr. Sci.*, 2011, **369**, 388.
44 D. J. Jones and J. Rozière, *J. Membr Sci.*, 2001, **185**, 41.
45 C. Zhao, H. Lin, K. Shao, X. Li, H. Ni, Z. Wang and H. Na, *J. Power Sources*, 2006, **162**, 1003.
46 E. Sengül, H. Erdener, R. G. Akay, H. Yücel, N. Baç and İ. Eroğlu, *Int. J. Hydrog. Energy*, 2009, **34**, 4645.
47 C. Wang, D. W. Shin, S. Y. Lee, N. R. Kang, G. P. Robertson, Y. M. Lee and M. D. Guiver, *J. Mater Chem.*, 2012, **22**, 25093.
48 H. Xie, D. Tao, X. Xiang, Y. Ou, X. Bai and L. Wang, *J. Membr Sci.*, 2015, **473**, 226.
49 B. Bae, T. Yoda, K. Miyatake, H. Uchida and M. Watanabe, *Angew. Chem., Int. Ed*., 2010, **49**, 317.
50 J. T. Lai, D. Filla and R. Shea, *Macromolecules*, 2002, **35**, 6754.
51 W. S. Hummers and R. E. Offeman, *J. Am. Chem. Soc.*, 1958, **80**, 1339.
52 Z. Liu, X. Duan, G. Qian, X. Zhou and W. Yuan, *Nanotechnology*, 2013, **24**, 045609.
53 T. Jiang, T. Kuila, N. H. Kim, B. C. Ku and J. H. Lee, *Comp. Sci. Technol.*, 2013, **79**, 115.
54 N. Yeole, S.N. R. Kutcherlapati and T. Jana, *J. Colloid. Inter. Sci*., 2015, **443**, 137.
55 Y. S. Ye, W. Y. Chen, Y. J. Huang, M. Y. Cheng, Y. C. Yen, C. C. Cheng and F. C. Chang, *J. Membr. Sci.*, 2010, **362**, 29.
56 L. Liu, C. Tong, Y. He, Y. Zhao and C. Lü, *J. Membr Sci.*, 2015, **487**, 99.
57 Y. Yang, X. Song, L. Yuan, M. Li, J. Liu, R. Ji and H. Zhao, *J. Polym. Sci. Part A: Polym. Chem.*, 2012, **50**, 329.
58 H. Erothu, J. Kolomanska, P. Johnston, S. Schumann, D. Deribew, D. T. W. Toolan, A. Gregori, C. D. -Lartigau, G. Portale, W. Bras, T. Arnold, A. Distler, R. C. Hiorns, P. M. -Tabari, T. W. Collins, J. R. Howse and P. D. Topham. *Maromolecules*, 2015, **48**, 2107.
59 H. Tang, G. J. Ehlert, Y. Lin and H. A. Sodano, *Nano Lett.*, 2012, **12**, 84.
60 H. Zarrin, D. Higgins, Y. Jun, Z. Chen and M. Fowler, *J. Phys. Chem. C*, 2011, **115**, 20774.
61 Y. Heo, H. Im and J. Kim, *J. Membr Sci.*, 2013, **425-426**, 11.
62 Y. J. Huang, Y. S. Ye, Y. J. Syu, B. J. Hwang and F. C. Chang, *J. Power Sources*, 2012, **208**, 144.
63 K. M. Beers and N. P. Balsara, *ACS Macro. Lett.*, 2012, **1**, 1155.
64 Z. Bai and T. D. Dang, *Macromol. Rapid. commun.*, 2006, **27**, 1271.
65 S. Feng, K. Shen, Y. Wang, J. Pang and Z. Jiang, *J. Power Sources*, 2013, **224**, 42.
66 H. Jiang, X. Guo, G. Zhang, J. Ni, C. Zhao, Z. Liu, L. Zhang, M. Li, S. Xu and H. Na, *J. Power Sources*, 2013, **241**, 529.
67 C. Y. Tseng, Y. S. Ye, M. Y. Cheng, K. Y. Kao, W. C. Shen, J. Rick, J. C. Chen and B. J. Hwang, *Adv. Energy Mater.*, 2011, **1**, 1220.
68 J. X. Leong, W. R. W. Dand, M. Ghasemi, A. Ahmad, M. Ismail and K. B. Liew, *Int. J. Hydrog. Energy*, 2015, **40**, 11604.
69 L. Geng, Y. He, D. Liu, X. Dai and C. Lü, *Micropor. Mesopor. Mater.*, 2012, **148**, 8.
70 D. S. Kim, B. Liu and M. D. Guiver, *Polymer*, 2006, **47**, 7871.
71 Z. Jiang, X. Zhao, Y. Fu and A. Manthiram, *J. Mater. Chem.*, 2012, **22**, 24862.
72 N. Li, S. Li, S. Zhang and J. Wang, *J. Power Sources*, 2009, **187**, 67.
73 C. H. Lee, K. A. Min, H. B. Park, Y. T. Hong, B. O. Jung and Y. M. Lee, *J. Membr Sci.*, 2007, **303**, 258.